Archives of Biochemistry and Biophysics 482 (2009) 17–24

Contents lists available at ScienceDirect

Archives of Biochemistry and Biophysics

journal homepage: www.elsevier.com/locate/yabbi

# Lipid-induced conformation of helix 7 from the pore-forming domain of the *Bacillus thuringiensis* Cry4Ba toxin: Implications for toxicity mechanism

Kasorn Tiewsiri [a,1], Wolfgang B. Fischer [b], Chanan Angsuthanasombat [a,*]

[a] Laboratory of Molecular Biophysics and Structural Biochemistry, Institute of Molecular Biology and Genetics, Mahidol University, Salaya Campus, Nakornpathom 73170, Thailand
[b] Institute of Biophotonics, School of Biomedical Science and Engineering, National Yang-Ming University, Taipei 112, Taiwan

ARTICLE INFO

*Article history:*
Received 19 August 2008
and in revised form 25 November 2008
Available online 10 December 2008

*Keywords:*
ATR-FTIR
Conserved aromatic residue
Cry δ-endotoxin
$H^+/D^+$ exchange
MD simulations
Zwitterionic membranes

ABSTRACT

Helix 7 in the Cry4Ba-pore-forming domain contains conserved $Tyr^{249}$ and $Phe^{264}$ that are crucially involved in mosquito-larvicidal activity. We have now characterized lipid-induced conformation of a 27-residue Cry4Ba-α7 peptide in phospholipid membranes using ATR-FTIR and hydrogen/deuterium ($H^+/D^+$) exchange experiments. ATR-FTIR results showed that conformation of this peptide is influenced by lipid composition and peptide–lipid ratio. For zwitterionic membranes, 1,2-dimyristoyl-*sn*-glycero-3-phosphocholine (DMPC) or 1,2-didecanoyl-*sn*-glycero-3-phosphocholine, the peptide adopted both α-helix and α-structure, but only α-helical conformation was observed in anionic membranes (1,2-dimyristoyl-*sn*-glycero-3-phosphoglycerol). $H^+/D^+$ exchange results showed protection of ~90% in DMPC for β-form, while α-helical form was found preferentially on membrane surface with both critical aromatic residues pointing towards bilayers. Analysis of 10-ns simulations of Cry4Ba-α7 in DMPC supports the stability of α-helical and β-conformations for membrane-associated and membrane-inserted states, respectively. We suggest that this lipid-induced conformational change of α7 is conceivably related to pore-forming mechanism as structural requirement for efficient membrane insertion.



Cry δ-endotoxins produced from *Bacillus thuringiensis* (*Bt*) are cytolytic pore-forming toxins, which are highly diverse and primarily target insect larvae [1]. For instance, the 130-kDa Cry4Ba toxin made by *Bt* subsp. *israelensis* is specifically toxic to mosquito-larvae of the genus *Aedes* and *Anopheles* which are human disease vectors transmitting pathogens for dengue hemorrhagic fever and malaria, respectively [2].

These *Bt* insecticidal proteins are synthesized as insoluble inactive protoxins in the form of crystalline inclusions that are solubilized and subsequently activated by gut proteases in the larval midgut lumen [2]. The activated toxins bind to specific receptors located on apical membranes of larval midgut epithelial cells and possibly undergo conformational changes and oligomerisation. One hypothesis is that this is followed by membrane insertion and pore formation, leading to osmotic cell lysis and eventual death of the larvae (for reviews, see [2,3]), although recent studies have proposed a different mechanism by which the toxin disrupts the signaling pathways of the cell [4]. However, the actual underlying mechanism of function remains to be investigated.

X-ray crystallographic data of almost all the major specificity classes of Cry δ-endotoxins, including the mosquito-specific Cry4Aa and Cry4Ba toxins [5,6], reveal a common topology with three distinct domains. Of particular interest, the N-terminal seven-helix domain (domain I) in which the relatively hydrophobic α5 is encircled by six other amphipathic helices has been shown to be responsible for ion-leakage pore formation [7].

Currently, substantial evidence supports an "umbrella-like" model that has been proposed to describe the membrane-bound state of the *Bt* Cry toxins. This model involves an insertion of α4 and α5 into the lipid bilayers as a helical hairpin structure, with the remaining helices spreading over the membrane surface [8]. A number of mutational studies suggested that α4 is aligned so that it faces the pore lumen and participates in ion conduction [9,10], while α5 interacts with the lipid membrane and is involved in toxin oligomerization [11,12]. This mode of action has been strengthened by our findings that one highly conserved tyrosine residue in the α4–α5 loop of the two closely related mosquito-specific toxins (Cry4Aa: $Tyr^{202}$; Cry4Ba: $Tyr^{170}$) is an important determinant for larvicidal activity, conceivably being involved in an interaction with lipid head groups for stabilizing the oligomeric pore structure [13,14]. We have further provided direct evidence for membrane-perturbing activity of the α4-loop-α5 hairpin isolated from the Cry4Ba toxin [15]. More recently, we have also provided pivotal evidence for the first time that the activated Cry4Ba toxin in association with DMPC lipid membranes could exist in at least two different trimeric conformations, conceivably implying the closed and open states of the pore [16]. Further investigation

* Corresponding author. Fax: +66 2 4419906.
*E-mail address:* stcas@mahidol.ac.th (C. Angsuthanasombat).
[1] Present address: Department of Entomology, Cornell University, Geneva, NY 14456-0462, USA.

0003-9861/$ - see front matter © 2009 Published by Elsevier Inc.
doi:10.1016/j.abb.2008.11.025

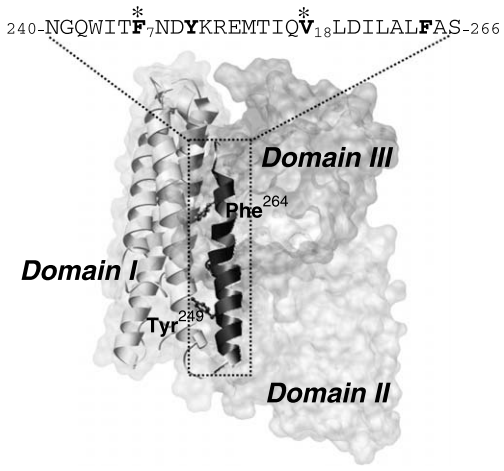


**Fig. 1.** Cry4Ba-helix 7 and its location in the activated toxin structure. Ribbon and surface representation of the Cry4Ba crystal structure with domain I (schematic ribbon) and domains II–III (surface model). Helix 7 (highlighted) within domain I shows the locations of the two critical aromatic residues, $Tyr^{249}$ and $Phe^{264}$ (ball and stick model). Sequence of the synthetic peptide corresponding α7 is illustrated above the structure. Nitrile-derivatised (C≡N) side-chain at $Phe^{7}$ and isotopic labeling at with $C^{13}{=}O^{18}$ $Val^{18}$ (corresponding to the positions $Phe^{246}$ and $Val^{257}$, respectively) are indicated by ∗. The structure was generated by using Chimera program.

for more details of the lipid-associated toxin conformation would be of great interest.

In addition, a refined model for the toxicity mechanism of the Cry toxins further suggested that α7 may serve as a binding sensor that could initiate the binding of the pore-forming domain to the lipid membrane, facilitating the membrane insertion of the α4–α5 pore-lining hairpin [8]. As was shown by numerous studies, the binding of membrane-inserting proteins to the lipid membrane surface via an aromatic cluster is a prerequisite for their membrane insertion and pore formation [17–19]. More recently, we have identified functional elements of Cry4Ba-α7 by demonstrating that two highly conserved aromatic residues, $Tyr^{249}$ and $Phe^{264}$, which are oriented on the same side of the helix (see Fig. 1) play an important role in toxin activity [20]. Notwithstanding the lack of membrane interaction and insertion studies, these two critical aromatic residues may indeed be the essential functional elements of α7, which could serve as a membrane-binding sensor to trigger the structural rearrangement of the pore-forming domain prior to membrane insertion.

In this study, ATR-FTIR[2] was employed to determine the conformation and spatial orientation of a synthetic peptide corresponding to α7 of Cry4Ba when reconstituted in different types of phospholipid membranes i.e. DMPC, DDPC and DMPG. As a complementary approach to experiments, MD simulation trajectories for a fully hydrated DMPC-α7 system were generated to study the structural stability of the peptide in association with the membrane at the microscopic level. In summary, the results suggest that α7 could exist in either as an α-helix on the membrane surface or a membrane-inserted β-hairpin.

[2] *Abbreviations used:* ATR-FTIR, attenuated total reflection-Fourier transform infrared; *Bt*, *Bacillus thuringiensis*; Ch, cholesterol; Cry, crystal; DDPC, 1,2-didecanoyl-*sn*-glycero-3-phosphocholine; DMPC, 1,2-dimyristoyl-*sn*-glycero-3-phosphocholine; DMPG, 1,2-dimyristoyl-*sn*-glycero-3-phosphoglycerol; DMSO, dimethylsulfoxide; FSD, Fourier self-deconvoluted; $H^+/D^+$, hydrogen/deuterium; LC-ESI-MS, liquid chromatography–mass spectrometry; LUVs, large unilamellar vesicles; MD, molecular dynamics; PC, phosphatidylcholine; PE, phosphatidylethanolamine; P/L, peptide-to-lipid molar ratio; RP-HPLC, reverse-phase high-performance liquid chromatography; SD/MD, simulated annealing via restrained molecular dynamics; TFA, trifluoroacetic acid.

## Materials and methods

### *Peptide preparation and purification*

A 27-residue Cry4Ba-α7 synthetic peptide (see Fig. 1), with isotopically labeled $C^{13}{=}O^{18}$ at $Val^{18}$ and nitrile-derivatised (C≡N) side-chain at $Phe^{7}$ (corresponding to the positions $Val^{257}$ and $Phe^{246}$, respectively) as internal local environment markers, was purchased from W.M. KECK Foundation Biotechnology Resource Laboratory, Yale University. Purification of the α7 peptide was accomplished by a reverse-phase high-performance liquid chromatography (RP-HPLC) system using a Jupiter $C_{18}$ column (3-μm particle size, 120-Å pore size, 4 × 50 mm, Phenomenex, USA). Chromatographic separation was achieved with a linear gradient of *B* in *A* (A = 0.05% TFA in $H_2O$; *B* = 0.05% TFA/20% $H_2O$/80% acetonitrile). Liquid chromatography–mass spectrometry (LC-ESI–MS) was employed to verify the purity of the α7 peptide.

The purified peptide (300 μg, lyophilized powder) was resuspended in each lipid solution (DMPC, DDPC and DMPG in hexafluoroisopropanol), resulting in a peptide–lipid ratio of 1:5, 1:30 and 1:100 (mol/mol). An aliquot of each mixture (5–10 μl) was applied onto one surface of a trapezoidal germanium (Ge) internal reflection element of 50 × 2 × 20 mm (Graseby Specac, Kent, UK) and dried using a dry $N_2$ stream, resulting in a multibilayer film (as evidenced by a decline in dichroic ratios for methylene stretching) [21]. For hydration under $D_2O$ and $H^+/D^+$ exchange experiments, spectra were collected after flushing the interior of the sample cell with $D_2O$-saturated $N_2$, obtained by bubbling dry $N_2$ through two compartments containing $D_2O$ for 1 h.

### *ATR-FTIR measurements*

IR spectra were collected from a Nicolet Nexus 470 spectrometer purged with $N_2$ and equipped with a MCT/A detector cooled with liquid $N_2$. Typically, interferograms were recorded with 4 $cm^{-1}$ spectral resolution with a 25-reflection ATR accessory (Graseby Specac) and a wire grid polariser (0.25 μm, Graseby Specac), A total 200 interferograms were averaged for one spectrum using 1-point zero filling and Happ-Genzel apodisation using either parallel (0°) or perpendicular (90°) polarised light.

Spectra were collected either after removal of bulk water or after hydration with $D_2O$ as described previously [21]. Briefly, in the first case, the dichroic ratio ($R^{ATR}$) of the amide I band (C=O stretching) and the band at 2850 $cm^{-1}$, derived from the $CH_2$ stretching of the lipid, was recorded. In the second case, after hydration with $D_2O$, $R^{ATR}$ of the amide A band (N–H stretching) was also recorded. Dichroic ratios were calculated as the ratio between the integrated absorptions collected from parallel and perpendicular polarised light.

### *ATR-FTIR data analysis*

Secondary structure of a peptide in the lipid membrane environment was determined using the corrected ATR spectra which were obtained from the parallel (||) and perpendicularly (⊥) polarised spectra, according to 1 (||) + 1.44 (⊥) as described previously [21]. The amide I band was Fourier self-deconvoluted (FSD) with a full-width at a half-height of 20 $cm^{-1}$ and an enhancement factor *k* of 2.0. Peak integration for the amide I was performed on these FSD spectra from 1700 to 1600 $cm^{-1}$. For the amide A band and the band at 2850 $cm^{-1}$, integration was performed without FSD from 3400 to 3200 $cm^{-1}$ and from 2890 to 2800 $cm^{-1}$, respectively.

Helix tilt ($\beta$) was calculated from the order parameters ($S$) for the helix $S_{helix}$ and the lipid $S_{lipid}$ [22] according to the following formula:

$$S = \frac{\epsilon_x^2 - R^{ATR}\epsilon_y^2 + \epsilon_z^2}{\epsilon_x^2 - R^{ATR}\epsilon_y^2 - 2\epsilon_z^2} \div \frac{3\cos^2\alpha - 1}{2} \quad (1)$$

$$S_{helix}\prime = \frac{S_{helix}}{S_{lipid}} \quad (2)$$

$$S_{helix}\prime = \frac{3\cos^2\alpha - 1}{2} \quad (3)$$

$R^{ATR}$ is the dichroic ratio of amide I or amide A (for $S_{helix}$) and the dichroic ratio of the 2850 $cm^{-1}$ band (for $S_{lipid}$). The angle $\alpha$ is 90° for the lipid symmetric $CH_2$ stretching, 39° for the peptidic C=O bond and 29° for the N-bond [22]. The parameters (electric field components of the evanescent wave) $\varepsilon_x = 1.398$, $\varepsilon_y = 1.516$ and $\varepsilon_z = 1.625$ are the integrated absorption coefficients for a Ge reflection element. Since the thickness of the final film sample was roughly estimated to be more than 10 μm, while the amplitude of the evanescent wave decays (at $1/\varepsilon$ at its initial value) after 1 μm in a Ge plate, the values for these components are those given by [23] according to a thick-film approximation.

$H^+/D^+$ exchange was calculated from the ratio of amide II to amide I, before and after the exchange using the corrected ATR spectra that were obtained as mentioned earlier.

*Peptide/bilayer/water simulating system and MD simulations*

Helical and β-structure models of the 27-residue α7 peptide were generated by simulated annealing via restrained molecular dynamics (SD/MD) using Xplor [24] and What if programs [25]. The conformation of the α-helical model was obtained from the Cry4Ba atomic coordinates [5]. For the β-conformation, it was predicted to be a β-hairpin based on the Chou-Fasman method [26] and the most stable configuration was selected after equilibrating in the lipid environment for 1 ns.

For the helical form lying at the lipid–water interface, the system contains 243 DMPC (initial set-up 288 DMPC molecules) and 12,199 water molecules (the SPC model) with a $Na^+$ ion added at the position corresponding to the lowest Coulomb energy of the ion. In peptide-orientation setup details, the helical model was oriented perpendicular to the bilayer normal, with its $Phe_{CN}^7$ side-chain pointing towards to the hydrophobic core of the lipid membrane according to ATR-FTIR experiments. On the other hand, the β-hairpin model was embedded transversely in a pre-equilibrated lipid bilayer (128 DMPC solvated in 6108 SPC water molecules) such that its long axis was parallel to the bilayer normal. Unfavorable lipid–protein contact made necessary for the removal of 32 DMPC molecules, giving a final total of 96 lipid molecules. Each

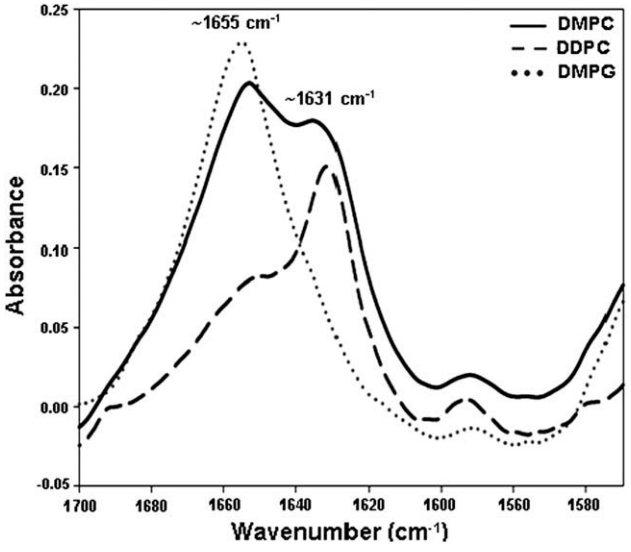


**Fig. 2.** ATR-FTIR spectra of the amide I band for the Cry4Ba-α7 peptide in different phospholipid bilayers. The α7 peptide (labeled with $C^{13}{=}O^{18}$ at $Val^{18}$ and C≡N side-chain at $Phe^7$) was reconstituted in DMPC (—), DMPG (----) and DDPC (….) lipids at a peptide-to-lipid molar ratio of 1:5.

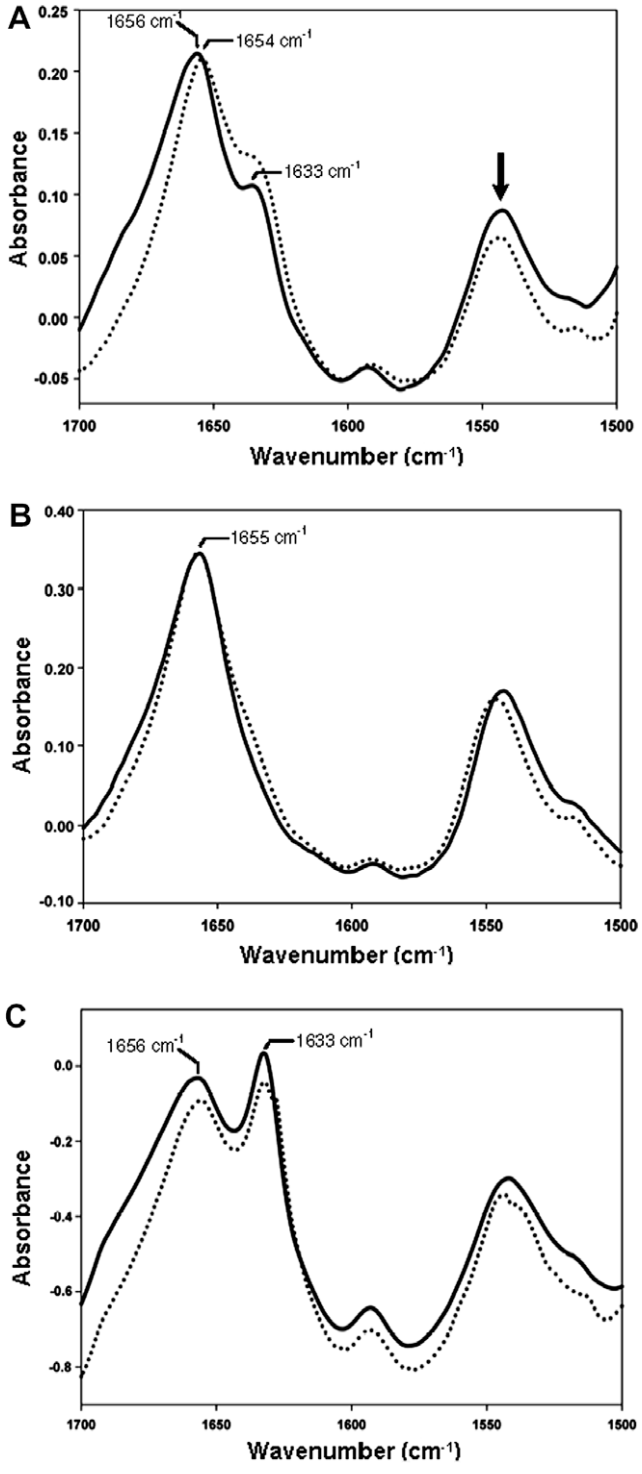


**Fig. 3.** ATR-FTIR spectra of the amide I and II of the Cry4Ba-α7 peptide in $H^+/D^+$ exchange experiments. The spectra corresponding to the amide I and II before (solid line) and after (dotted line) hydration with $D_2O$ of the Cry4Ba-α7 peptide in DMPC (A), DMPG (B) and DDPC (C) membranes at a peptide-to-lipid molar ratio of 1:30. The peptide used was labeled with $C^{13}{=}O^{18}$ at $Val^{18}$ and C≡N side-chain at $Phe^7$. The reduction in amide II intensity due to $H^+/D^+$ exchange is indicated by an arrow.

**Table 1**
Estimated percentage of secondary structure contents of the Cry4Ba-α7 peptide in DMPC, DMPG and DDPC with different peptide-to-lipid ratios.

| Secondary structure (%)[a] | | | | | | |
|---|---|---|---|---|---|---|
| Sample (peptide-to-lipid) | DMPC | | DMPG | | DDPC | |
| | α-Helix | β-Sheet | α-Helix | β-Sheet | α-Helix | β-Sheet |
| Helix 7 (1:5) | 50 | 50 | 100 | – | 23 | 77 |
| Helix 7 (1:30) | 65 | 35 | 100 | – | 43 | 57 |
| Helix 7 (1:100) | 90 | 10 | 100 | – | 87 | 12 |

[a] Standard deviation of each value is <5%.

system was minimized and equilibrated for 400 ps prior to unrestrainted MD simulations.

MD simulations were performed using the program package GROMACS 3.2.1 software (http://www.gromacs.org), employing an NPT ensemble (i.e., constant number of particles, pressure and temperature) with a time-step simulation of 2 fs. The simulated pressure was 1 bar, and the temperature was 300 K. Anisotropic pressure-coupling [27] in $x-$, $y-$ and was employed so that the area per lipid was allowed to be adjusted during the simulations. The Berendsen temperature-coupling was carried out with a coupling constant of 0.1 ps. LINCS algorithm [28] were used to keep all bond lengths constrained. Long-range electrostatic interactions were calculated using the particle-mesh Ewald method [29]. Lennard-Jones and short-range Coulombic interactions were cut off at 1.0 nm.

*Peptide-induced liposome perturbation assays*

Large unilamellar vesicles (LUVs) were prepared from 2 mg/ml of a mixture of lipids (Avanti Polar Lipid, USA) of phosphatidylcholine (PC)/phosphatidylethanolamine (PE)/cholesterol (Ch) (10:10:1 w/w) dissolved in chloroform. The solvent was evaporated under a $N_2$ stream and the resulting lipid film was resuspended in 200 μl of 60 mM calcein (pre-dissolved in 100 mM $Na_2CO_3$, pH 9.0)/10 mM Tris–HCl, pH 9.0. After subjected to five cycles of freezing and thawing, the lipid suspension was repeatedly squeezed through a polycarbonate membrane (0.1 μm pore size, Avanti Polar Lipid) for a minimum of 20 passes, using a two-syringe extruder (Avanti Polar Lipid) to yield LUVs with a mean diameter of about 100 nm. The untrapped calcein was removed from the LUV suspension by gel filtration on a HiTrap™ desalting column (Amersham Pharmacia Biotech, Uppsala, Sweden). Liposome concentrations were estimated by measuring the lipid phosphorus content [30], and a final concentration of 1.25 μM LUV was used for the calcein release assay [31]. After adding 5 μl of a peptide sample (5–10 μg dissolved in dimethylsulfoxide, DMSO) into 400 μl of LUV solution placed in a 1 cm light-path polymethyl methacrylate cuvette (Brand, Germany), resulting in a peptide–lipid ratio of 1:20. The degree of LUV perturbation was determined as increase in the fluorescence intensity of the released calcein. Fluorescence was monitored at 25 °C on a Perkin–Elmer LS50 spectrofluorimeter with excitation and emission wavelengths set at 485 and 520 nm, respectively, and a slit width of 5 nm.

## Results and discussion

The "umbrella-like" model which has been widely used to describe the membrane-bound state of the Cry δ-endotoxins suggests that α-helix 7 could serve as a membrane-binding sensor to facilitate the structural rearrangement of the pore-forming domain, thus promoting the membrane insertion of the α4-loop-α5 pore-lining segment [8]. In our earlier studies, we have made a single-proline substitution in α7 of the Cry4Ba toxin, and found that the integrity of α7 conceivably plays a role in toxicity [32]. More recently, we have strengthened the functional significance of α7 by showing that the highly conserved aromaticity of $Tyr^{249}$ and $Phe^{264}$ within this helix plays an important role in larvicidal activity of the Cry4Ba toxin [20]. To gain a more critical insight into the role of this conserved helix in toxicity mechanism, a 27-residue synthetic peptide corresponding to the Cry4Ba-α7 (see Fig. 1) was structurally and functionally characterized with respect to its interaction with the lipid membrane.

*Conformation of Cry4Ba-7 in different lipid membranes*

ATR-FTIR spectroscopy was employed to determine the peptide structure of Cry4Ba-α7 when reconstituted in three different types of phospholipid multibilayers, i.e. zwitterionic (DMPC or DDPC) and negatively charged (DMPG) phospholipids. As shown in Fig. 2, the frequencies of the amide I region of the α7 peptide after mixing with DMPC at peptide-to-lipid molar ratio (P/L) of 1:5 showed two major absorption peaks at 1654 and 1633 $cm^{-1}$ that are assigned to α-helical and β-sheet structures, respectively. This indicates that the 27-residue α7 peptide could adopt both α-helical and β-conformations in a DMPC membrane-bound state. However, only one major amide I absorption peak of the peptide was found centered at 1655 and 1631 $cm^{-1}$ when mixed with DMPG and DDPC, respectively, indicating that the peptide reconstituted in DMPG is mainly α-helical, while the peptide within DDPC adopts predominantly a β-structure. Thus, conformation of the Cry4Ba-α7 peptide is essentially influenced by the lipid composition. Likewise, it has been shown via solid-state nuclear magnetic resonance that the type of phospholipids plays an important role in the conformation of the transmembrane-phospholamban peptide in lipid bilayers [33].

Other earlier studies have shown that the neuropeptide substance P in the presence of POPG shows an α-helix conformation at low P/L but adopts a β-sheet structure at high P/L (>1:40) [34]. It has also been shown for the Alzheimer β-amyloid peptide which undergoes conformational changes in POPG vesicles from a β-structure to an α-helical structure upon increasing the peptide concentration [35]. In this regard, we also conducted experiments to explore an effect of the change in P/L on the peptide structure of Cry4Ba-α7. Table 1 lists the relative distribution of the secondary structure elements for the α7 peptide observed in various conditions. For DMPC at P/L of 1:100, the portion of the α-helical structure was enhanced (∼90%) when compared to P/L of 1:30 (∼65%) and of 1:5 (∼50%) while the β-structure decreased in the same direction. A similar behavior was also found when the peptide was mixed with DDPC membranes (see Table 1). However, the peptide adopts only α-helical conformation when reconstituted in the anionic DMPG membrane for all three P/L ratios. The peptide was α-helical for all three types of lipids at P/L of 1:100, indicating that this peptide is rather stable in an α-helical conformation at a high lipid concentration, independently from the lipid environments.

*Orientation of the 7 peptide within multibilayer phospholipid membranes*

Further quantitative analysis was performed to determine the orientation and membrane insertion of the Cry4B-α7 peptide when reconstituted in DMPC, DMPG and DDPC membranes. As described earlier with ATR-FTIR, the percentage of membrane-inserted residues can be determined by measuring the amide I/amide II ratio before and after hydration with $D_2O$ [21] and the orientation of the peptide can be obtained from the dichroic ratios of amide I or amide A bands [36].

The amide II absorption band (1544 $cm^{-1}$) for the α7 peptide in DMPC membranes was still present after 1-h exposure to $D_2O$

**Table 2**
Orientation analysis of the Cry4Ba-α7 peptide in DMPC, DMPG and DDPC at peptide-to-lipid molar ratio of 1:30.

| Lipid systems | Bulk water removed ($H_2O$) | | Hydrated membrane ($D_2O$) | | | | | |
|---|---|---|---|---|---|---|---|---|
| | $R_{AI}$ | $R_{AA}$ | $R_{AI}$ | $R_{AA}$ | $R_{ISO}$ | Exchanged (%) | | β° |
| | | | | | | α-Hairpin | β-Hairpin | |
| DMPC | 1.5 ± 0.2 | 1.8 ± 0.1 | 1.8 ± 0.01 | 1.6 ± 0.1 | 1.8 ± 0.1 | 60 ± 7.1 | 10 ± 4.2 | 65° ± 2.6 |
| DMPG | 3.7 ± 0.1 | 2.0 ± 0.2 | 2.6 ± 0.1 | 2.0 ± 0.2 | 3.2 ± 0.06 | 4 ± 3.2 | – | 37° ± 4.9 |
| DDPC | 1.7 ± 0.1 | 1.5 ± 0.1 | 1.1 ± 0.05 | 1.6 ± 0.05 | 1.2 ± 0.04 | 52 ± 6.4 | 9 ± 6.4 | 53° ± 4.9 |

Dichroic ratios of amide I ($R_{AI}$), of amide A ($R_{AA}$) and of isotopic labeling $C^{13}{=}O^{18}$ ($R_{ISO}$) are shown. $R_{AI}$ is the dichroic ratio from the formation of α-helix. β° represents an average tilt angle of α-helical peptides in DMPC, DDPC and DMPG at a peptide-to-lipid ratio of 1:30. Exchanged (%) refers to the percent part of the peptides that are not protected from $D_2O$ exchange, calculated from $R_{AI}$ or $R_{AA}$ (within parentheses). The data is the average of three independent experiments.

(Fig. 3A, arrow), indicating that part of the peptide molecule is protected from the $D_2O$ exchange and embedded in the lipid membrane. Moreover, examination of the ratio between non-polarized amide II and amide I before and after $D_2O$ exchange revealed that ~90% of the β-form peptide was inserted in the DMPC membrane, while only ~40% of the α-helical form did not exchange in $D_2O$. In similar experiments using DMPG or DDPC membranes, the percentage of non-exchanged amide groups was ~95% for the α-helical form in DMPG (Fig. 3B), and ~91% and ~50% for the β-helical conformations, respectively, in DDPC (Fig. 3C).

The orientation of the α7 peptide with respect to the lipid membrane was obtained from the dichroic ratios of amide I or amide A bands (see Table 2). It is noteworthy that the dichroic ratio of the band at 2850 $cm^{-1}$ from the methylene $CH_2$ stretching of DMPC, DMPG and DDPC reconstituted with the peptide was found to be 1.1, 1.2 and 1.1, respectively, indicating that all the phospholipid membranes used under experimental conditions are typically well-ordered bilayers [21]. For the α-helical form peptide in DMPC, after hydration in $D_2O$, the dichroism of the amide I ($R_{AI}$ = 1.8) suggested that the non-exchange part of this conformation was not inserted in, but rather lying mostly parallel to, the membrane surface. The helix tilt of the helical form in the anionic phospholipid (DMPG) was ~43° to the membrane normal, with the amide A dichroic ratio ($R_{AA}$) of 2.0. In addition, when the shorter-acyl-chain phospholipid (DDPC) was employed, the amide I band dichroism of the α7 peptide indicated that the α-helix was most likely on the membrane surface ($R_{AI}$ = 1.1). However, for the orientation of the β-sheet structure, it remains a challenge for experimental approaches to provide a more reliable way in determination of the tilt angle since the β-form is not an axially-symmetric structure.

The α7 peptide was also isotopically labeled with $C^{13}{=}O^{18}$ at $Val^{18}$ (see Fig. 1) to obtain site-specific orientational information [37,38]. The isotope-edited peak appeared at ~1591 $cm^{-1}$ which is red-shifted from the amide I band (Fig. 4, arrow). As seen in Table 2, the site-specific dichroic ratios ($R_{ISO}$) calculated for the $C^{13}{=}O^{18}$ isotope-labeled peptide in all three different lipid membranes are consistent with the data from the $H^+/D^+$ exchange experiments, albeit significantly greater for the case in DMPG ($R_{ISO}$ = 3.2). This give the same trend of the orientational information of the α7 peptide in the lipidic environment obtained from the amide I or amide A bands.

To further determine the spatial orientation of individual side-chains, particularly for the two toxicity important residues – $Tyr^{249}$ and $Phe^{264}$ [20], the C≡N stretching vibration of the nitrile-derivatised $Phe^7$ ($Phe_{CN}$, see Fig. 1) in the α7 peptide was employed as an infrared environmental probe [39]. If the derivatised side-chain is entirely hydrated, the C≡N stretching band is centered at 2235 $cm^{-1}$, while buried in the hydrophobic milieu of the lipid bilayer, this band shifts to 2229 $cm^{-1}$ [39,40]. The nitrile-derivatised peptide reconstituted in any of the membranes used here exhibited a C≡N band at ~2228 $cm^{-1}$ (data not shown). This is indicative of hydrophobic environment, i.e., the $Phe_{CN}$ side-chain of the α7 peptide is buried in the hydrophobic core of the lipid membrane. Thus, $Phe^7$ ($Phe_{CN}$), $Tyr^{10}$ and $Phe^{25}$ (corresponding to $Tyr^{249}$ and $Phe^{264}$, respectively, see Fig. 1) are all located on the same side of the α-helical peptide and therefore point towards the bilayer membrane.

At this stage, our ATR-FTIR studies reveal that both structural conformation and insertion behaviors of the Cry4Ba-α7 peptide in either DMPC or DDPC are rather similar, exhibiting a helical conformation laying on the membrane surface and a β-structure penetrating into the lipid membrane. The insect cell membranes are primarily composed of zwitterionic phospholipids such as phosphatidylcholine (PC) and phosphatidylethanolamine (PE) [41,42]. Thus, this lipid-induced β-conformation observed in only zwitterionic DMPC and DDPC membranes, which are more relevant to the target cell membranes than DMPG, might have a functional role in toxicity. The two critical aromatic residues ($Tyr^{249}$ and $Phe^{264}$) in α7 may play a role in toxin-membrane interaction needed for such lipid-induced conformational transition prior to an efficient membrane insertion and pore formation of the Cry4Ba toxin.

*Structure and dynamics of the Cry4Ba-7 peptide in model bilayers*

MD simulations of the α7 peptide in an explicit DMPC bilayer were carried out to study the dynamics of the peptide in both its α-helical and β-sheet conformations. Unlike the α-helical conformation which is taken from the Cry4Ba crystallographic structure

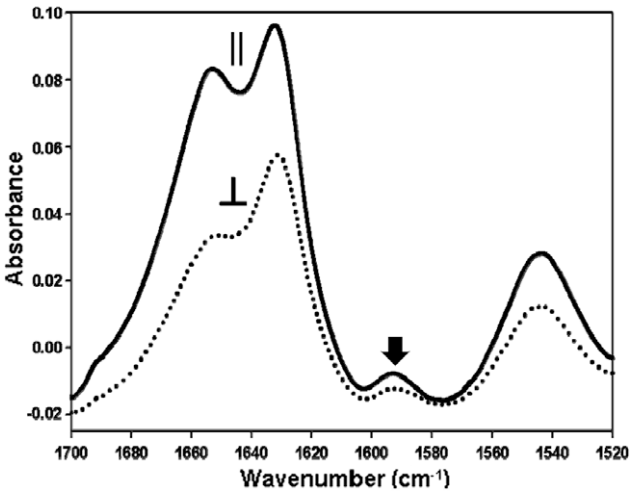


**Fig. 4.** ATR-FTIR spectra of the Cry4Ba-α7 peptide collected from parallel and perpendicular polarized light. The spectra of the Cry4Ba-α7 peptide (labeled with $C^{13}{=}O^{18}$ at $Val^{18}$ and C≡N side-chain at $Phe^7$) in DMPC membranes, recorded using 0° (solid line) or 90° (dotted line) polarization. The isotope-edited peak is indicated by an arrow.

[5], the β-conformation which is assumed to be a β-hairpin was derived from the most stable configuration. In accord with the ATR-FTIR data (see Table 1), the α-helical form was oriented parallel to the membrane–water interface with the $Phe_{CN}^{7}$ side-chain facing the hydrophobic milieu of the membrane, while the β-hairpin model was inserted transversely into the membrane with its long axis parallel to the bilayer normal.

Fig. 5 shows the results of MD simulation trajectories for a fully hydrated DMPC-α7 system. An overall measure of the structural stability of the DMPC-associated α7 peptide in each model system was obtained by comparing the time-dependent $C_\alpha$ atoms of root mean square deviations (RMSD) from its starting structure (Fig. 5A). For the α-helical model simulations, the RMSD rises within the first 1 ns to a level of about 0.18 ± 0.04 nm. The β-hairpin model levels off after 2 ns and adopts a value of 0.35 ± 0.05 nm (average for $t$ = 2 to 10 ns). This value is likely due to the arrangement of the amino acid side-chains so that the polar and charged residues would compensate the unfavorable side-chains in the low dielectric core of the lipid bilayer. In addition, analysis of the time evolution of secondary structures reveals that α-helicity of this DMPC-associated helical conformation is largely preserved throughout the 10-ns simulations (Fig. 5B). Likewise, in the β-hairpin model simulations, the initial β-conformation is retained primarily in residues 7–13 and 20–27 throughout the period of simulations (Fig. 5C).

To visualize the structural change and orientation of each conformation of the DMPC-associated α7 peptide, snapshots of the MD simulation trajectories are illustrated in Fig. 6. The 10-ns MD trajectories for the α-helical conformation (Fig. 6A and B) reveal that this helical peptide remains located at the lipid–water interface, tilted with respect to the horizontal membrane plane by ~90° (see Fig. 6B). In the simulations starting with the β-hairpin conformation inserted into the bilayer (Fig. 6C and D), the model remains in its conformation in respect to the lipid membrane during the duration of simulation (Fig. 6D). Particularly for the α-helical conformation, such behavior is in good agreement to that of previously observed for the Cry3Aa-α7 peptide that cannot undergo voltage-dependent insertion into lipid bilayers in MD simulation studies [43] or is preferentially oriented nearly parallel to the membrane surface in Monte Carlo simulations [8].

Other studies with the bacterial toxin pneumolysin have shown that there is a conformational transition from the membrane-bound pre-pore to the transmembrane pore by the substantial refolding of α-helical regions into membrane-inserted β-hairpins [44]. It has also been shown that the hydrophobic stretch (PLVG) at the apex of the transmembrane β-hairpin plays a crucial role in driving the mem-

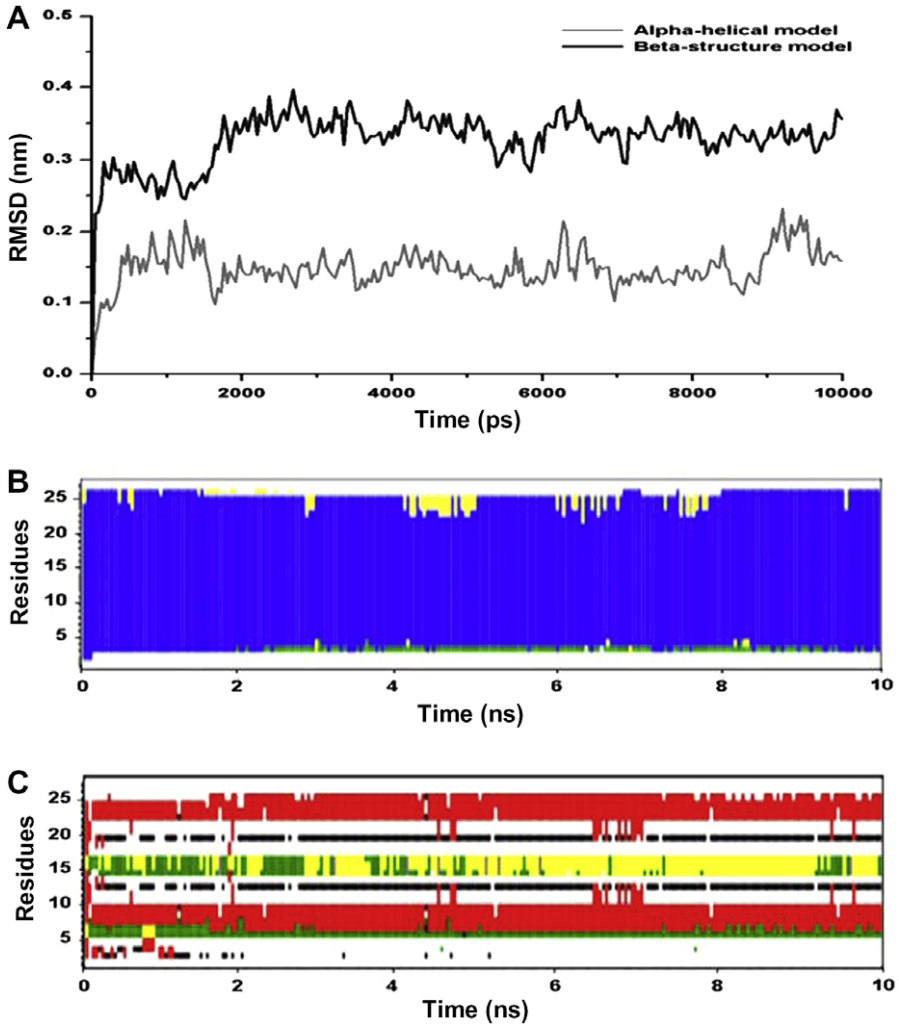


**Fig. 5.** MD simulation trajectories of the Cry4Ba-α7 peptide in DMPC bilayers. (A) The root mean square deviation (RMSD) versus time for the $C_\alpha$ atoms in α-helical model or β-structure model. Secondary structures of the Cry4Ba-α7 peptide, analysed using DSSP as a function of simulation time for the α-helical form located at the membrane–water interface region (B) and the β-form inserted transversely into the DMPC bilayers (C). Grayscale: blue, α-helix; yellow, turn; red, β-sheet; green, bending; black, β-bridge.

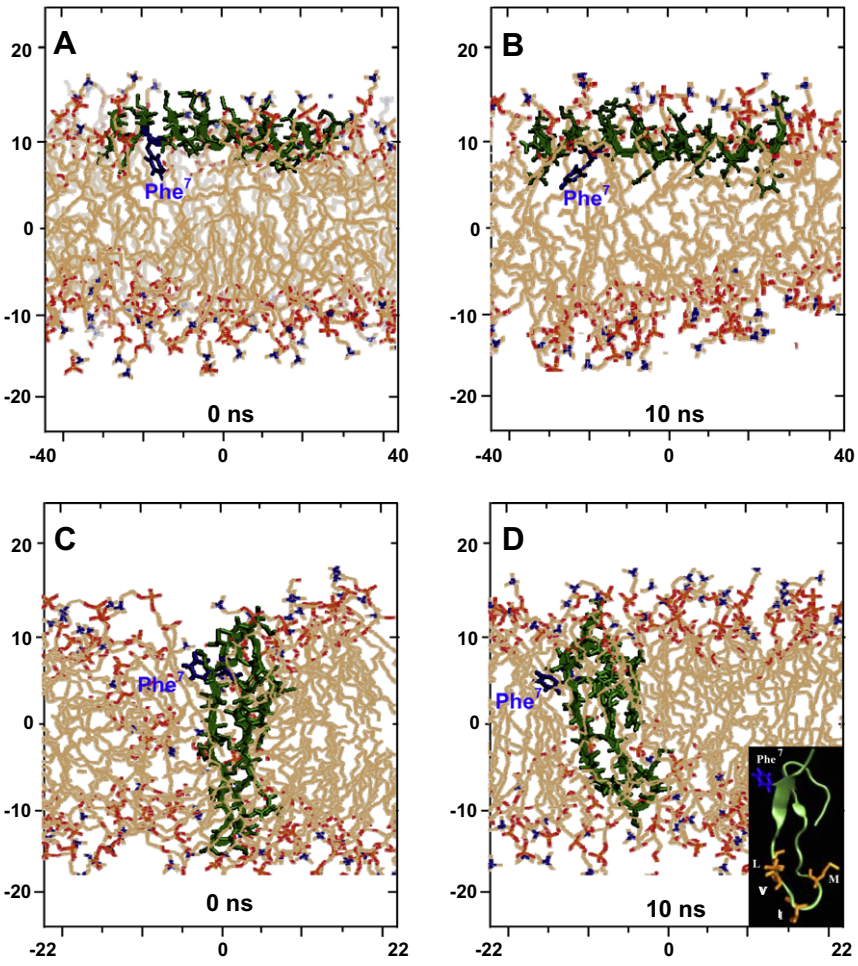


**Fig. 6.** MD snapshots of two conformations of the Cry4Ba-α7 peptide in DMPC bilayers. Snapshots of the MD trajectories of the Cry4Ba-α7 peptide in a fully hydrated DMPC system at simulation times 0 and 10 ns for the membrane-associated helical model (A and B), and for the membrane-inserted β-hairpin model (C and D). $Phe^{7}$ side-chain is indicated and colored in blue. Inset of D illustrates its ribbon model with the hydrophobic turn, $Met^{14}$, $Ile^{16}$, $Val^{18}$ and $Leu^{19}$.

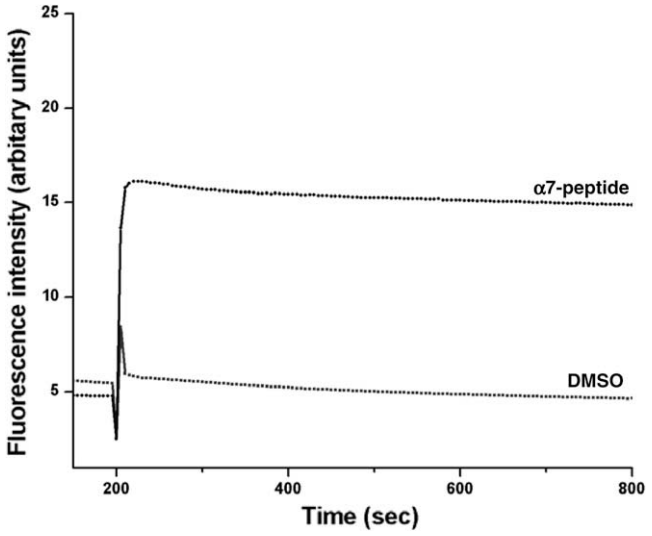


**Fig. 7.** Effects the Cry4Ba-α7 peptide on calcein release from LUVs. The fluorescence intensity of the entrapped calcein upon release from LUVs, which were continuously monitored as a function of time after incubation with the Cry4Ba-α7 peptide (dissolved in DMSO) at a peptide-to-lipid molar ratio of 1:20 (▲). Four microlitres of DMSO was used as a negative control (●).

brane insertion of the aerolysin pore-forming toxin [45]. This may conceivably reflect our results that α-helix 7 in the Cry4Ba pore-forming domain might be able to refold into an extended β-hairpin with the hydrophobic turn (M-I-VL, see Fig. 6D, inset) to insert into the lipid membrane, albeit the hairpin containing several charged and polar-uncharged residues that are energetically unfavorable for membrane insertion. We thus propose that this β-conformation induced by an interaction with zwitterionic lipid membranes would possibly impart greater ability to the Cry toxin molecule to protrude the transmembrane helical hairpin, i.e. α4-loop-α5 from the bundle to act as an initiator of membrane penetration.

*Membrane perturbation induced by the Cry4Ba-7 peptide*

To further validate the potential effect of the α7 peptide on the integrity of lipid membranes, entrapped dye-release experiments were carried out to access peptide-induced perturbation of liposomes. Herein, LUVs of PC/PE/Ch compositions, which are more biologically relevant to the insect cell membranes, were created with self-quenched fluorescence dye, i.e. calcein, entrapped in their interior cavity. The release of the entrapped calcein from LUVs was measured as the 'dequenching' of the calcein fluorescence, and was thereby monitored continuously as an increase in the fluorescence intensity. Under the conditions used in the assays, the α7 peptide (~2 μM) was able to perturb the lipid packing and cause leakage of the encapsulated calcein (see Fig. 7). We, however, noted that

the membrane-perturbing activity of α7 is much lower than that of the proposed transmembrane pore-lining hairpin, i.e. α 4-loop-α5 (~0.6 μM), as reported previously [15]. As can be inferred from the ATR-FTIR and MD simulations studies, the α7-induced disruption of PC/PE/Ch vesicles could possibly be caused by either a membrane-associated α-helical form or a membrane-inserted β-hairpin. Electrostatic interactions between the phospholipid headgroups and the charges within the α-helical form lining on the membrane surface as well as the membrane penetration of the β-hairpin conformation could lead to some extent of perturbation of the membrane integrity, causing leakage of vesicular contents.

In conclusion, our ATR-FTIR studies have provided pivotal evidence for the first time that the Cry4Ba-α7 peptide when reconstituted into zwitterionic phospholipids could adopt either an α-helical conformation that prefers a membrane surface location or a β-structure with a membrane-inserted orientation. Conceivably, the lipid-induced β-conformation of α7 might serve as a lipid anchor needed for an efficient insertion of the pore-forming Cry toxin into the bilayer membrane. However, it remains a challenge for experimental approaches, including FRET (fluorescence resonance energy transfer)-based method, DSC (differential scanning calorimetry) or ITC (isothermal titration calorimetric) studies, to provide more structural and functional details of the Cry4Ba-α7 peptide interacting with the lipid bilayer membranes. Further simulations exploring the possibility of dynamic refolding of this helix between a membrane-associated α-helical form and a membrane-inserted β-hairpin are also of great interest since this would shed light on toxicity mechanism of the Cry insecticidal proteins.

## Acknowledgments

We are grateful to Dr. Jaume Torres (School of Biological Sciences, Nanyang Technological University, Singapore) for making available facilities in ATR-FTIR studies and critical comments. Support for this work has been generously funded by the Thailand Research Fund (TRF) in cooperation with the Commission of Higher Education (to C.A.). The Royal Golden Jubilee Ph.D. scholarship from TRF (to K.T.) is gratefully acknowledged.

## References

[1] R.A. De Maagd, A. Bravo, N. Crickmore, Trends Genet. 17 (2003) 193–199.
[2] E. Schnepf, N. Crickmore, J.V. Rie, D. Lereclus, J. Baum, J. Feitelson, D.R. Zeigler, D.H. Dean, Microbiol. Mol. Biol. Rev. 62 (1998) 775–806.
[3] M.E. Whalon, B.A. Wingerd, Arch. Insect Biochem. Physiol. 54 (2003) 200–211.
[4] X. Zhang, M. Candas, N.B. Griko, R. Taussig, L.A. Bulla, Proc. Natl. Acad. Sci. USA 103 (2006) 9897–9902.
[5] P. Boonserm, P. Davis, D.J. Ellar, J. Li, J. Mol. Biol. 348 (2005) 363–382.
[6] P. Boonserm, M. Min, C. Angsuthanasombat, J. Lescar, J. Bacteriol. 188 (2006) 3391–3401.
[7] T. Puntheeranurak, P. Uawithya, L. Potvin, C. Angsuthanasombat, J.L. Schwartz, Mol. Membr. Biol. 21 (2004) 67–74.
[8] E. Gazit, P. La Rocca, M.S.P. Samson, Y. Shai, Proc. Natl. Acad. Sci. USA 95 (1998) 12289–12294.
[9] L. Masson, B.E. Tabashnik, Y.B. Liu, R. Brousseau, J.L. Schwartz, J. Biol. Chem. 274 (1999) 31996–32000.
[10] I. Sramala, S. Leetachewa, C. Krittanai, G. Katzenmeier, S. Panyim, C. Angsuthanasombat, J. Biochem. Mol. Biol. Biophys. 5 (2001) 219–225.
[11] M. Nunez-Valdez, J. Sánchez, L. Lina, L. Güereca, A. Bravo, Biochim. Biophys. Acta 1546 (2001) 122–131.
[12] S. Likitvivatanavong, G. Katzenmeier, C. Angsuthanasombat, Arch. Biochem. Biophys. 445 (2006) 46–55.
[13] Y. Kanintronkul, I. Sramala, G. Katzenmeier, S. Panyim, C. Angsuthanasombat, Mol. Biotechnol. 24 (2003) 11–19.
[14] W. Pornwiroon, G. Katzenmeier, S. Panyim, C. Angsuthanasombat, J. Biochem. Mol. Biol. 37 (2004) 292–297.
[15] S. Leetachewa, G. Katzenmeier, C. Angsuthanasombat, J. Biochem. Mol. Biol. 39 (2006) 270–277.
[16] P. Ounjai, V.M. Unger, F.J. Sigworth, C. Angsuthanasombat, Biochem. Biophys. Res. Commun. 361 (2007) 890–895.
[17] P. Braun, G. Von Heijne, Biochemistry 38 (1999) 9778–9782.
[18] P. Malovrh, G. Viero, M.D. Serra, Z. Podlesek, J.H. Lakey, P. Macek, G. Menestrina, G. Anderluh, J. Biol. Chem. 278 (2003) 22678–22685.
[19] A. Drechsler, C. Potrich, J.K. Sabo, M. Frisanco, G. Guella, M. Della Serra, G. Anderluh, F. Separovic, R.S. Norton, Biochemistry 45 (2006) 1818–1828.
[20] K. Tiewsiri, C. Angsuthanasombat, J. Biochem. Mol. Biol. 40 (2007) 163–171.
[21] D. Marsh, Biophys. J. 77 (1999) 2630–2637.
[22] C.S.B. Chia, J. Torres, M.A. Cooper, I.T. Arkin, J.H. Bowie, FEBS Lett. 512 (2002) 47–51.
[23] N. Harrick, Internal Reflection Spectroscopy, Interscience Publishers, 1967.
[24] A.T. Brünger, X-PLOR Version 3.1: A System for X-ray Crystallography and NMR, Yale University Press, 1992.
[25] G. Vriend, J. Mol. Graph. 8 (1990) 52–56.
[26] P.Y. Chou, G.D. Fasman, Adv. Enzymol. Relat. Areas Mol. Biol. 47 (1978) 45–148.
[27] H.J.C. Berendsen, J.P.M. Postma, W.F.V. Gunsteren, A. Dinola, J.R. Haak, J. Chem. Phys. 81 (1984) 3684–3690.
[28] B. Hess, H. Bekker, H.J.C. Berendsen, J. Fraaije, J. Comput. Chem. 18 (1997) 1463–1472.
[29] U. Essmann, L. Perera, M.L. Berkowitz, T. Darden, H. Lee, L.G. Pedersen, J. Chem. Phys. 103 (1995) 8577–8593.
[30] R.J. Mrsny, J.J. Volwerk, O.H. Griffith, Chem. Phys. Lipids 39 (1986) 185–191.
[31] T.M. Allen, L.G. Cleland, Biochim. Biophys. Acta 597 (1980) 418–426.
[32] I. Sramala, P. Uawithya, U. Chanama, S. Leetachewa, C. Krittanai, G. Katzenmeier, S. Panyim, C. Angsuthanasombat, J. Biochem. Mol. Biol. Biophys. 4 (2000) 187–193.
[33] E.S. Karp, E.K. Tiburu, S. Abu-Baker, G.A. Lorigan, Biochim. Biophys. Acta 1758 (2006) 772–780.
[34] A. Seelig, T. Alt, S. Lotz, G. HÖlzemann, Biochemistry 35 (1996) 4365–4374.
[35] E. Terzi, G. HÖlzemann, J. Seelig, Biochemistry 36 (1997) 14845–14852.
[36] I.T. Arkin, W.P. Russ, M. Lebendiker, S. Schuldiner, Biochemistry 35 (1996) 7233–7238.
[37] J. Torres, A. Kukol, J.M. Goodman, I.T. Arkin, Biopolymers 59 (2001) 396–401.
[38] I.T. Arkin, Curr. Opin. Chem. Biol. 10 (2006) 394–401.
[39] M.J. Tucker, Z. Getahun, V. Nanda, W.F. De Grado, F. Gai, J. Am. Chem. Soc. 126 (2004) 5078–5079.
[40] J. Torres, K. Parthasarathy, X. Lin, R. Saravanan, A. Kukol, D.X. Liu, Biophys. J. 91 (2006) 938–947.
[41] K. Marheineke, S.L. Grünewald, W. Christie, H. Reiländer, FEBS Lett. 441 (1998) 49–52.
[42] G.C. Atella, M. Shahabuddin, J. Exp. Biol. 205 (2002) 3623–3630.
[43] P.C. Biggin, M.S.P. Sansom, Biophys. Chem. 60 (1996) 99–110.
[44] S.J. Tilley, E.V. Orlova, R.J.C. Gilbert, P.W. Andrew, H.R. Saibil, Cell 121 (2005) 247–256.
[45] I. Iacovache, P. Paumard, H. Scheib, C. Lesieur, N. Sakai, S. Matile, M.W. Parker, F.G. Van der Goot, EMBO J. 25 (2006) 457–466.